LANGMUIR

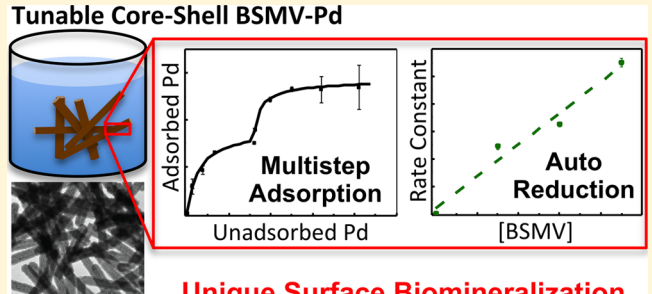
BSMV as a Biotemplate for Palladium Nanomaterial Synthesis

Oluwamayowa O. Adigun, Erin Lynn Retzlaff-Roberts, Gloria Novikova, Longfei Wang, Bong-Suk Kim, Jan Ilavsky, Jeffrey T. Miller, L. Sue Loesch-Fries, and Michael T. Harris

[†]School of Chemical Engineering, Purdue University, 480 Stadium Mall Drive, West Lafayette, Indiana 47907, United States [‡]Department of Botany and Plant Pathology, Purdue University, 915 West State Street, West Lafayette, Indiana 47907, United States §X-ray Science Division, APS Argonne National Laboratory, 9700S Cass Avenue, Lemont, Illinois 60439, United States

Supporting Information

ABSTRACT: The vast unexplored virus biodiversity makes the application of virus templates to nanomaterial synthesis especially promising. Here, a new biotemplate, Barley stripe mosaic virus (BSMV) was successfully used to synthesize organic-metal nanorods of similarly high quality to those produced with Tobacco mosaic virus (TMV). The mineralization behavior was characterized in terms of the reduction and adsorption of precursor and nanocrystal formation processes. The BSMV surface-mediated reduction of Pd⁽²⁺⁾ proceeded via first-order kinetics in both Pd⁽²⁺⁾ and BSMV. The adsorption equilibrium relationship of PdCl₃H₂O⁻ on the BSMV surface was described by a multistep Langmuir isotherm suggesting



Unique Surface Biomineralization

alternative adsorbate-adsorbent interactions when compared to those on TMV. It was deduced that the first local isotherm is governed by electrostatically driven adsorption, which is then followed by sorption driven by covalent affinity of metal precursor molecules for amino acid residues. Furthermore, the total adsorption capacity of palladium species on BSMV is more than double of that on TMV. Finally, study of the BSMV-Pd particles by combining USAXS and SAXS enabled the characterization of all length scales in the synthesized nanomaterials. Results confirm the presence of core-shell cylindrical particles with 1-2 nm grains. The nanorods were uniform and monodisperse, with controllable diameters and therefore, of similar quality to those synthesized with TMV. Overall, BSMV has been confirmed as a viable alternate biotemplate with unique biomineralization behavior. With these results, the biotemplate toolbox has been expanded for the synthesis of new materials and comparative study of biomineralization processes.

INTRODUCTION

Directed synthesis of nanomaterials with controllable dimensions remains a subject of immediate concern in nanotechnology.^{1,2} Biotemplating, the use of naturally occurring biomolecules to develop nanomaterials of similar morphology, hierarchical complexity and nanometric precision, is a viable means to easily and inexpensively produce needed nanomaterials on a large scale.3 Specifically, the use of viruses as biotemplates has been pursued as a potent solution due to their unique advantages for applications in catalysis, 4–7 nanocircuitry, 8–10 chemical sensing, 11–13 biocatalysis, 14 memory devices, 15 and light harvesting. 16,17 As many studies of the M13 bacteriophage and the Tobacco mosaic virus (TMV) have shown, virus templates are particularly exciting due to the wide range of chemical interactions afforded by their multifunctional protein surfaces. The potential presence of polar, hydrophilic, charged, acidic, and basic functionalities on a single template allow the formation of a wide range of inorganic nanoparticles. Thus, noble metals, $^{9,18-25}$ bimetallic materials, 26 and semiconductors^{27,28} have been mineralized on viruses.

When considered in the context of the numerous virus species on the planet, the vast range of possibilities for new materials from such biodiversity still remains unexplored.²⁹ TMV, M13, and their engineered variants, remain the prevalent biotemplates employed in attempted nanowire and nanorod synthesis. The expansion of the biotemplate toolbox will enable comparative examination of fundamental processes controlling mineralization such as precursor adsorption, reduction, and nanocrystal growth. We have previously reported the hydrothermal synthesis of nanorods, which depended on autocatalytic reduction of Pd on the surface of the virus template rather than using an exogenous reducer. 18 Localization of biomineralization on the surface of the virus coat protein (CP) inherently produces nanowires that are dense, uniform, controllable, and monodisperse. 19 Nevertheless, even with much effort, 30,31 surface-mediated synthesis has not been successfully applied to reproduce high quality nanowires in other virus-metal systems.

We propose that the Barley stripe mosaic virus (BSMV) is a promising candidate to produce high quality nanomaterials.

Received: September 14, 2016 Revised: January 24, 2017 Published: January 24, 2017



The biological activity of BSMV in host cells has been well-studied over the last three decades. Moreover, its physiochemical and structural characteristics have recently been elucidated at 4.1 Å resolution. BSMV virions are rigid rods consisting of a tripartite positive sense ssRNA genome surrounded by CPs of 23 kDa. The particles (virions) are 20.8 or 21.4 nm in outer diameter, with an inner central channel of 4 nm. They are between 110 and 150 nm long, although particles are known to align end-to-end to produce much longer rods. Although They are between 110 and 150 nm long, although particles are known to align end-to-end to produce much longer rods. The BSMV CP tertiary structure, which is graphically depicted in Figure 1a, is similar to that of TMV CP

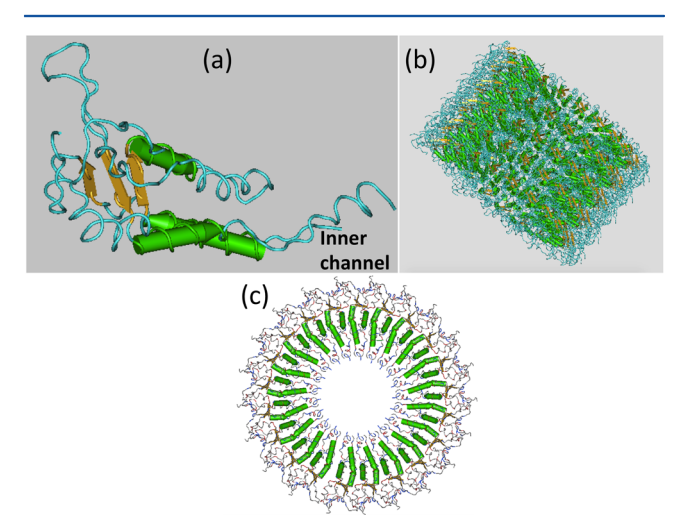


Figure 1. Graphical model of BSMV. (a) BSMV coat protein. (b) Side view of an assembled BSMV virion. Six turns around the RNA are shown. (c) Top-down view of a single turn of assembled BSMV coat proteins (without RNA). Green tubes indicate Alpha helices with N—C terminal direction. Blue wires are protein side chains and yellow sheets are protein strands. The red and blue regions seen in panel c indicate local positively and negatively charged regions of the coat protein. These are notably on the outside or inner hollow of the virus. Structure was obtained from ncmi pdb and MMDB database and was developed by Clare et al. ^{39,70}

as indicated by the presence and positioning of major alpha helices, and conservation of key amino acid residues.³⁹ These CPs assemble around an RNA to form a virion (or particle), which retains a structural integrity relevant for infectivity up to ~65 °C after 10 min. 43 Consequently, BSMV can potentially be applied to surface biomineralization, while retaining its mechanical robustness, as has been observed on TMV. Conversely, BSMV offers alternative biotemplating due to its different physiochemical properties (e.g., isoelectric point) and other active surface functionalities, which allow for different chemical interactions compared to TMV. For example, the BSMV CP has been reported to consist of two additional long insertions on the outer surface when compared to the TMV CP. One of these is a sequence of 10 amino acids (residues 1-10), located at the exposed N-terminus while the other (residues 84-94) is an insertion loop which also protrudes onto the outer surface.³⁹

This study demonstrates that BSMV is a viable biotemplate for mineralization of palladium (Pd) nanorods. Uniform BSMV-Pd nanorods at different coating densities were synthesized by the hydrothermal synthesis. *In situ* X-ray absorption spectroscopy (XAS), UV-vis spectroscopy, and ultra-small-angle X-ray scattering (USAXS) were used to

characterize the mineralization behavior through precursor adsorption, reduction, and nanoparticle growth.

METHODS AND PROCEDURES

BSMV Purification. BSMV purification was performed according to published protocols. ^{38,44}

Virus Coating Procedure. Virus coating was performed in a CSTR (3.5 mL) reactor vessel with temperature regulation via a heating block. Na₂PdCl₄ solution (usually between 0.2 mM and 3 mM) was added to the reactor containing a 2 mL virus solution (0.035 mg/mL) after it had been heated to the desired synthesis temperature in an eppendorf tube. During an ex-situ study (UV-vis characterization), 400 μ L aliquots of the solution were collected regularly. The ongoing interfacial phenomena (reactions, adsorption) in these aliquots were then immediately quenched by separation of the solid phase with Acrodisc Syringe Filters (Pall life sciences, 13 mm). The solid phase consists of noticeable (brown aggregates imaged with TEM) dispersions of Pd and virus particles. The filtrate solution was diluted 3-fold in water at 4 °C to further reduce interfacial activity. The absorbance of aliquots at 256 nm representing PdCl₃(H₂O) was measured at 25 °C by a UV-vis spectrophotometer (Varian Cary 100). Since adventitious reactions involving Pd complexes are minimal under these conditions, 45 the uptake of the dominant Pd species, PdCl₃(H₂O)⁻, was the difference between the concentrations of the aliquots (incubated with BSMV or TMV) and the concentration of the control (no virus). Adsorption experiments were performed over shorter times (within 150s) and 6-8 samples were collected during this period. For all adsorption experiments, a swift uptake was noticed and then a plateau was reached. The equilibrium concentration for adsorption processes was chosen as the concentration after 150 s. Pd reduction studies were performed in a similar manner but occurred over longer times (typically between 40 and 180 min). The quantitative adsorption and reduction studies (adsorption isotherms and reaction rate studies) reported in this paper were performed only during the first coating of Palladium, i.e., phenomena caused by interaction between Pd solution and virion outer surface. Further coating was performed by collecting particles, washing five times in 10 mL of water and then reincubating in 0.7 mM Na₂PdCl₄ solution. The continuous coating and adsorption procedure have been adopted from previous works.4

In situ X-ray Absorption Spectroscopy Experiments. In situ XAS experiments were conducted at the Advanced Photon Source (Argonne National Laboratory, Lemont, IL) 10 ID-B beamline. Pd precursor solution (3 mM Na₂PdCl₄) was placed in a continuously stirred 3 mL reactor with BSMV (0.15–0.5 mg/mL) and then into the path of X-rays. At the Pd K-edge (24.4 keV), spectra of the solution contents and reference materials (Pd foil and precursor solution) were taken in transmission mode. Each spectrum from the reaction was then analyzed individually, but identically. For the XANES analysis, each spectrum was fit as a linear combination of the two reference spectra using WINXAS software. EXAFS parameters were obtained by performing a least-square fit of a Fourier transformed k^2 -weighted normalized absorption spectra in R-space.

USAXS/SAXS Characterization and Analysis. Solutions containing nanorods were deposited between two glass slides and placed in the path of the X-rays. USAXS/SAXS scans of solutions (not dried samples) were taken. USAXS was performed using a Bonse-Hart camera at beamline 9ID-C at 21 keV. 49 SAXS data collection was done with a Pilatus camera. Standard data reduction was employed to obtain scattering curves for the scanned nanorods.

USAXS Modeling. The scattering vector is defined as

$$q = \frac{4\pi \sin \theta}{\lambda} \tag{1}$$

where θ is the scattering angle and λ is the wavelength of the incident beam of X-rays.

For the dilute core—shell cylinder population, particle scattering is defined $^{\rm 50}$ by

$$I(q) = \bar{N} \int_0^\infty D_{\rm n}(R_{\rm p}) P(q, R_{\rm p}) dR_{\rm p}$$
 (2)

where \overline{N} is the number concentration of particles, $R_{\rm p}$ is the outer radius of the nanorod. ⁵¹ $D_{\rm n}(R_{\rm p})$ is a distribution function so that $D_{\rm n}(R_{\rm p})$ d $R_{\rm p}$ represents the number of particles between $R_{\rm p}$ and $R_{\rm p}$ + d $R_{\rm p}$. $P(q_{\rm s}R_{\rm p})$ is the form factor for a core—shell cylinder given by

$$P(q, R_{\rm p}) = \frac{1}{V_{\rm p}} \int_0^{\pi/2} f^2(q, \alpha) \sin \alpha d\alpha$$
 (3)

where

$$f(q, \alpha) = 2(\rho_{\text{core}} - \rho_{\text{shell}}) V_{\text{cors}} j_0(qL \cos \alpha) \frac{J_1[qR_{\text{core}} \sin \alpha]}{(qR_{\text{core}} \sin \alpha)}$$

$$+ 2(\rho_{\text{shell}} - \rho_{\text{solvent}}) V_P j_0(qL \cos \alpha) \frac{J_1[qR_P \sin \alpha]}{(qR_P \sin \alpha)}$$
(4)

 α is the angle between the scattering vector and the cylinder axis. $\rho_{\rm core} = 9 \times 10^{-10} \ cm^{-2}, \, \rho_{\rm shell} = 89.3 \times 10^{-10} \ cm^{-2}$ and $\rho_{\rm solvent} = 12 \times 10^{-10} \ cm^{-2}$ represent the scattering length density of the core (virus), shell (Pd) and solvent (water) phases, respectively. $R_{\rm core}$ and $R_{\rm p}$ are the radii of the core and entire particle. L is the length of the particle. Then the core volume and total particle volume are

$$V_{\text{core}} = \pi R_{\text{core}}^{2} L, \quad V_{\text{p}} = \pi R_{\text{p}}^{2} L, \quad j_{0}(x) = \frac{\sin x}{x}$$

and $J_1(x)$ is the Bessel function of the first kind.

Assuming a uniform coating of Pd on the biotemplate, a distribution describing the thickness of the metal layer (shell) around the biotemplate (core) was defined as

$$D_{\rm n}(t) = D_{\rm n}(R_{\rm P} - R_{\rm core}) \tag{5}$$

Then, the growing Pd shell with a thickness (t) can be represented in the Gaussian distribution,

$$D_{\rm n}(t) = \frac{\exp\left[-\frac{(t-\mu_{\rm t})^2}{2\sigma^2}\right]}{\sigma\sqrt{2\pi}} \tag{6}$$

where μ_i is the mean of the shell thickness and σ is the standard deviation in the thickness.

The primary nanoparticles at high q were modeled by using the Beaucage unified equation,

$$I(q) = \left(G_1 \exp\left[-\frac{q^2 R_{g,1}^2}{3}\right] + B_1 \exp\left[-\frac{q^2 R_{g,1}^2}{3}\right] q^* {}_1(q)^{P_1}\right)$$
(7)

where

$$q^*_1 = \frac{q}{\left\{ \operatorname{erf}\left(\frac{qR_{g,i}}{\sqrt{6}}\right) \right\}^3}$$

and G_1 is the guinier prefactor, B_1 is the power law prefactor, R_g is the radius of gyration, and P_1 is the power law exponent.

RESULTS AND DISCUSSION

BSMV virions (Figure 2a) were coated with a dense, uniform layer of palladium nanoparticles using the expedient hydrothermal synthesis (Figure 2b). Nanoparticles were observed on the virus template after 20 min of incubation at 55 °C in a stirred tank reactor with 0.75 mM Na₂PdCl₄. Figure 3a shows that the first layer of Pd nanoparticles does not fully coat the biotemplate after 20 min of incubation. The Fourier transform of the high resolution transmission emission microscopy (HRTEM) image of this first layer of particles (inset of Figure 3a) indicates a lattice spacing of 0.22 nm, corresponding to the (111) crystalline facet of FCC metallic palladium. Therefore,

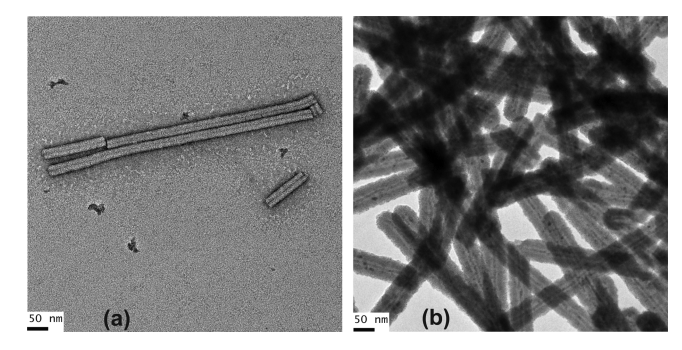


Figure 2. Transmission electron microscopy (TEM) images of BSMV and nanorods. (a) Purified BSMV virions negative stained with uranyl acetate; (b) BSMV-Pd nanorods collected after five coating cycles with Pd precursor. Extensive outer mineralization and inner surface (thin nanowire) mineralization is evident here.

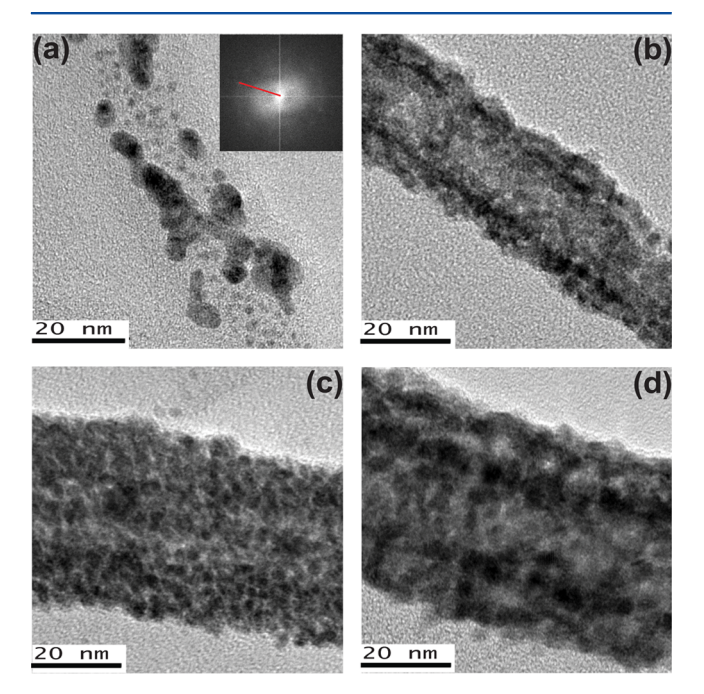


Figure 3. Transmission electron microscopy (TEM) images of single BSMV-Pd nanorods were collected after incubation of 0.02 mg/mL of BSMV in 0.75 mM of Na_2PdCl_4 . BSMV-Pd collected after (a) one coating cycle. Inset in shows the Fourier transform of a high resolution transmission electron microscopy (HRTEM) image of Pd nanoparticles: (b) two coating cycles; (c) five coating cycles; (d) six coating cycles.

the observed coating on the BSMV-Pd particles comprises of $Pd^{(0)}$. These particles, which consist of BSMV virions decorated with isolated small metal nanoparticles, can be applied in catalysis of organic reactions. The particles were precipitated, washed five times to remove residual salt, and recoated several times by reincubation in 0.75 mM Na_2PdCl_4 solution at 55 °C (Figure 3). As shown in Figure 3d, the BSMV-Pd diameter could be increased up to 56.8 ± 2.7 nm after 6 coatings. These results show that the exposed BSMV CP surface contained active subunits, which enabled surface-driven biomineralization of Pd. The biomineralization behavior of the first layer, which involves autoreduction of Pd on the BSMV surface, was studied more closely using UV—vis and *in situ* XAS.

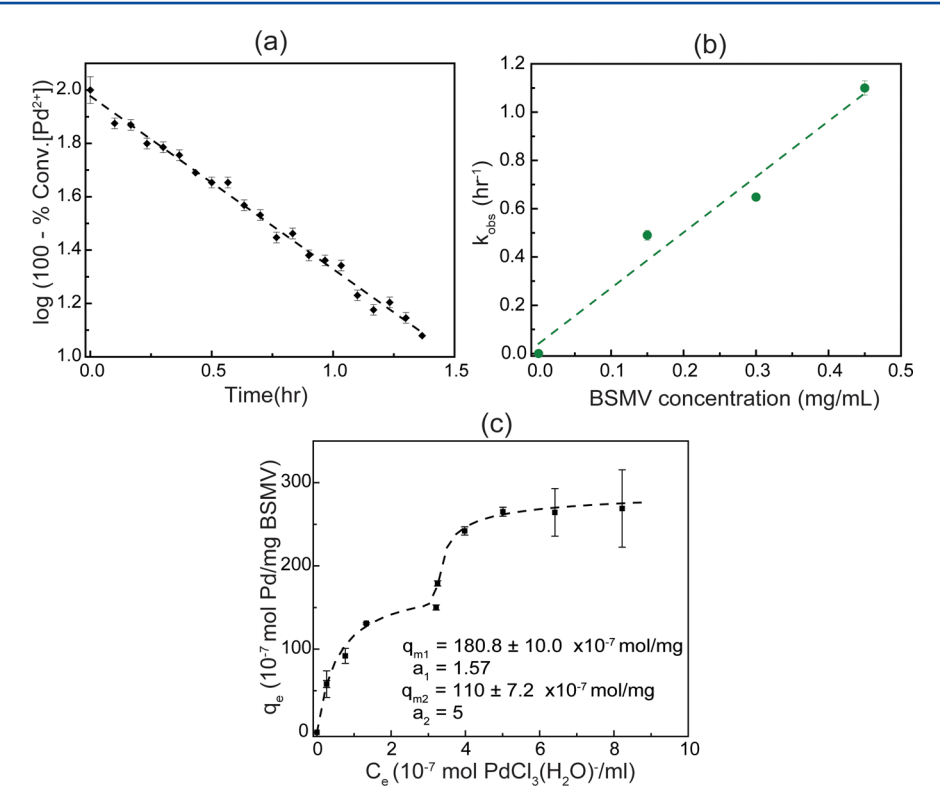


Figure 4. Mineralization of $PdCl_3(H_2O)^-$ on BSMV. (a) Fit of the concentration data to a first order kinetic model. Data was obtained from XAS characterization of the reduction of 3 mM $Pd^{(2+)}$ during interaction with 0.3 mg/mL BSMV at 55 °C. (b) Fit of kinetic parameter to BSMV concentration to obtain reaction order and intrinsic rate constant at 55 °C. Dashed lines (---) in (a) and (b) represent linear fits. (c) Adsorption of $PdCl_3(H_2O)^-$ onto BSMV at 25 °C. Adsorption isotherm was fit to a multistep Langmuir isotherm represented by dashed lines (---).

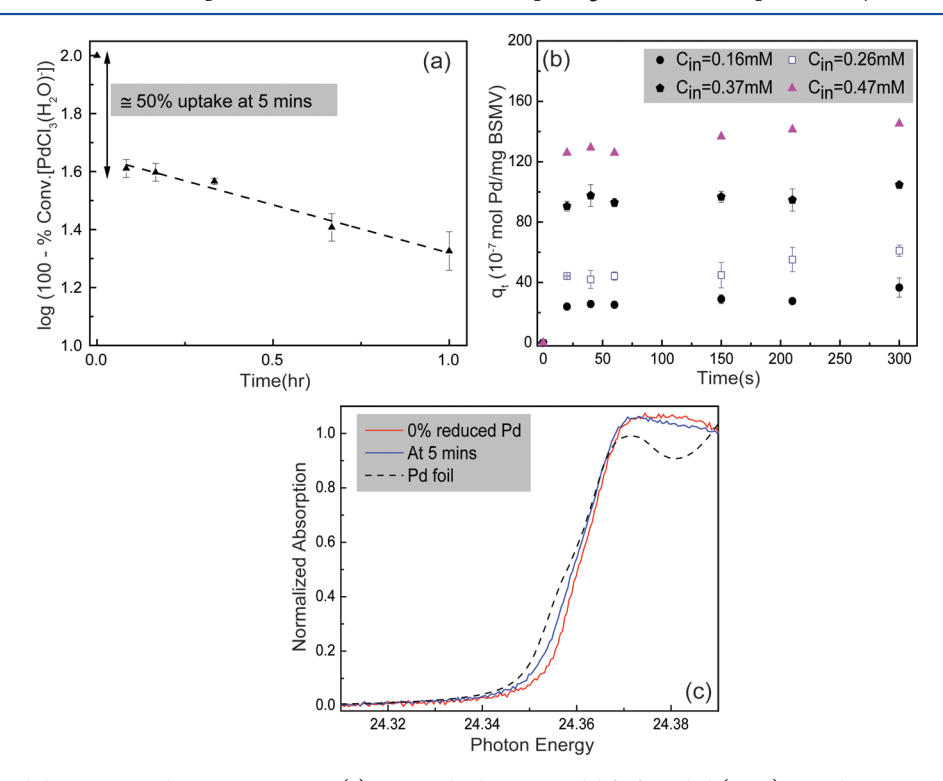


Figure 5. Changes in Pd during mineralization on BSMV. (a) First-order kinetic model fit for $PdCl_3(H_2O)^-$ uptake on BSMV determined by UV–vis spectroscopy. The obtained kinetic constant is identical to that obtained from XAS characterization under the same conditions (0.15 mg/mL BSMV, 57 °C). (b) Uptake of $PdCl_3(H_2O)^-$ at early times obtained by UV–vis absorbance experiments at 256 nm at 25 °C. Experiments were performed at six different $Pd^{(2+)}$ concentrations (four of them are shown here). (c) XANES spectra of Pd references and spectrum at 5 min after incubation at 57 °C.

In situ XAS analysis was performed with 3 mM Na₂PdCl₄ at 55 °C at four different concentrations of BSMV. Spectra were collected at the Pd K-edge (24.4 keV) over time.

A first-order reduction in Pd⁽²⁺⁾ was observed from analysis of the X-ray absorption near edge spectroscopy (XANES) region over time (Figure 4a). Efficient use of the expensive Pd precursor was indicated by the complete (>95%) reduction of Pd at the end of the synthesis. Figure 4b shows that the rate of reduction was a linear function of concentration. The negative control (no virus) signified that the presence of BSMV was required for the reduction of Pd⁽²⁺⁾. Thus, X-ray induced reduction was ruled as unlikely. Extended X-ray Absorption Fine Structure analysis of the precursor solution indicated a Cl coordination number of 3.2, thus agreeing with previous reports that $PdCl_3(H_2O)^-$ is the dominant (>85%) Pd species in the solution. 45,52 Therefore, the rate law for the reduction of Pd (Reaction I) on BSMV is given by eq 8. The obtained intrinsic rate constant (k) was $2.3 \pm 0.3 \text{ h}^{-1}$. Such surface-induced reduction indicates that the BSMV CP displays functionalities, or peptides which mediate the reduction of Pd species. This is corroborated by studies by Tan et al. which showed that peptides consisting of serine, threonine, arginine, glutamine, lysine, and tyrosine have higher reductive capability for AuCl4^{-,50}

$$PdCl_3(H_2O)^- + 2e^- \rightarrow Pd^{(0)} + 3Cl^- + H_2O$$
 (I)

$$\frac{\mathrm{d[Pd]}}{\mathrm{d}t} = k_{\mathrm{obs}}[\mathrm{Pd}^{2+}] = k[\mathrm{BSMV}][\mathrm{Pd}^{2+}]$$
(8)

where k_{obs} = k [BSMV], and k is the intrinsic rate constant associated with the reduction of Pd⁽²⁺⁾.

The uptake of PdCl₃(H₂O)⁻ by BSMV at 25 °C was determined by UV-vis spectroscopy (Figure 5). As seen in Figures 4a,b, there was a swift drop in concentration of PdCl₃(H₂O)⁻ within the first 20 seconds of incubation. This rapid uptake is followed by a much slower uptake, which can be fit to a first order reaction in PdCl₃(H₂O)⁻. XANES analysis (Figure 5c) indicates that, Pd⁽²⁺⁾ does not significantly reduce (<5% reduction) during the first 5 min of incubation. Therefore, the swift concentration drop represents the adsorption of PdCl₃(H₂O⁻), i.e., sorption without acquisition of reducing electrons. Furthermore, the adsorption behavior is observed to approach equilibrium very quickly (as seen in Figure 5b) enabling the decoupling of the two processes. Adsorption occurs within the first 20 seconds and then approaches thermodynamic equilibrium; conversely, the reduction of Pd occurs over a much longer time period (about a few hours). The thermodynamic adsorption behavior of BSMV was studied by incubating different concentrations of Pd with 7.5×10^{-2} mg/mL of BSMV at 25 °C. The saturation concentration was then assumed to be the equilibrium concentration for an adsorption process. By sampling the supernatant after separation of the solid phase, which comprises the virions with adsorbed Pd species, the equilibrium relationship between the virus surface and supernatant solution was obtained. Figure 4c shows that the adsorption behavior is best fit by a multistep Langmuir isotherm (eq9). In contrast, the adsorption behavior of PdCl₃(H₂O⁻) on TMV at equilibrium, is best fit by a single step Langmuir isotherm. 46

$$q_{e} = q_{m1} \frac{a_{1}C_{e}}{1 + a_{1}C_{e}} + q_{m2} \frac{a_{2}[(C_{e} - b) + |C_{e} - b|]}{2 + a_{2}[(C_{e} - b) + |C_{e} - b|]}$$
(9)

where q_e and C_e are the equilibrium concentration of adsorbing species on the virus and of solution respectively, $q_{\rm mi}$ represents the adsorption capacity, a_i is the adsorption intensity and b is the critical concentration limit for the initiation of the second isotherm step.

To further elucidate the adsorption behavior, it is important to note that the reported isoelectric points for BSMV and TMV are 4.5 and 3.5, respectively. 54,55 This means that the exposed outer surfaces have a net negative charge at pH 5. However, continuum electrostatics theories are not sufficient to describe adsorption behavior. 56 Table S1 shows that the BSMV virion surface consists of positively charged functionalities, which are absent on the TMV virion surface. Therefore, adsorption of PdCl₃(H₂O)⁻ on the TMV is solely driven by covalent interactions while adsorption on the BSMV surface is driven by both electrostatic and covalent interactions. This is further confirmed by the much faster kinetics (<20s in Figure 5b) on BSMV compared to TMV (≈150 s).46 Previous molecular dynamic and experimental studies indicate that when both electrostatic and covalent relationships are accessible, the electrostatic interactions generally govern inorganic adsorption due to greater interaction energies. 57,58 Ion exchange chromatography studies involving proteins consisting of Lys, His, and Arg also confirm this finding.⁵⁶ Adsorption is consequently best modeled by the multistep Langmuir isotherm 59,60 so that each of the sorbing relationships is represented by a local isotherm. The first local Langmuir isotherm is determined by ion-pairing between PdCl₃(H₂O)⁻ and positively charged sites on the virus surface.

From the amino acid residues present on the BSMV surface (N terminus (residues 1–13), C terminus (residues 191–198), and the insertion loop (residues 84-94), Lys9 and His13 are viable candidates for this kind of adsorption. 57,58 The adsorption capacity of 180.8 \pm 10 \times 10⁻⁷ mol Pd/mL describes this local isotherm. After the positively charged sites have been neutralized by the binding of the negatively charged Pd species, covalently driven affinity for Pd species will become dominant in the adsorption process. Favorable ligand switching between coordinated chlorine and surface amino acid residues will drive the adsorption. Prospective residues involved in this process include Asp₃, Ser₅, The₇, Glu₈, and Tyr₉₁, which display reported Pd⁽²⁺⁾ ligands such as hydroxyl, amines, or or aromatics⁶³ at the virion's outer surface. The observed adsorption capacity for the second local isotherm is 110 \pm 7.2×10^{-7} mol Pd/mL, resulting in a total adsorption capacity of 307.9 \pm 20 \times 10⁻⁷ mol Pd/mL for the BSMV template, which is more than double of that of TMV (127 \pm 10 \times 10⁻⁷ mol Pd/mL) under the same conditions. A higher adsorption capacity is particularly important in traditional electroless deposition where an external reducer is employed, because the degree of metallization is solely dependent on the adsorption process. Thus, we show that BSMV biotemplating will allow for greater metallization of metals when this synthetic approach is necessary, e.g., in biotemplating with Au, Ag, and Cu. Additionally, as the first report of a multistep adsorption behavior on a virus biotemplate, this study illustrates the advantage of using a multifunctionally diverse biotemplate for mineralization. Hence, sophisticated multifunctional materials can be created from the two sorbing interactions.

In order to study the particulate system, USAXS and SAXS were simultaneously used to monitor nanoparticle formation as new coatings were added to the BSMV-Pd nanorods. The large q range (0.0001 Å to 1.0 Å) afforded by combining both

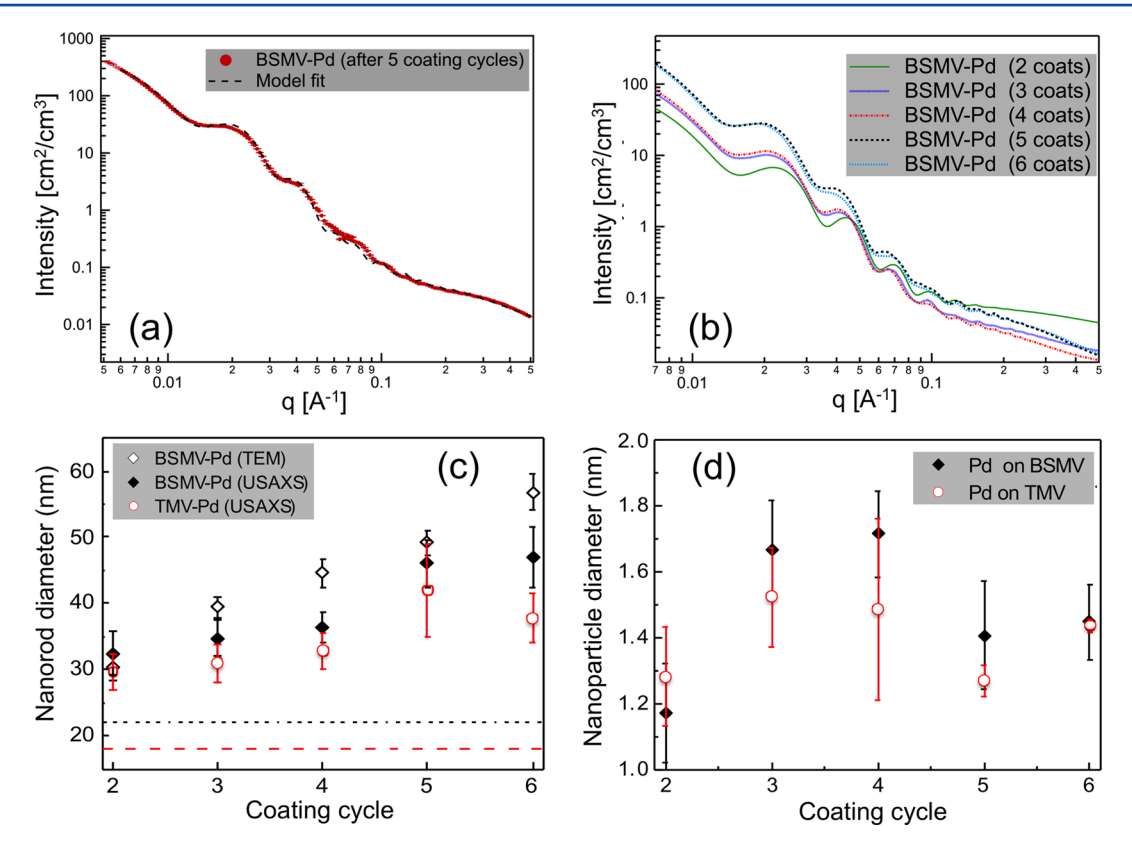


Figure 6. USAXS characterization of Pd coated biotemplates. (a) Log-log plot showing a typical fit of developed model to scattering of nanorods after solvent subtraction. Here, BSMV coated 5 times with Pd is shown. (b) Fitted curves for BSMV-Pd from 2 to 6 coatings of Pd. After 1 coating cycle, nanoparticles did not scatter significantly. Fitted curves for TMV-Pd scattering are shown in Figure S2b. (c) Nanorod diameters from coreshell fit for BSMV-Pd and TMV-Pd, and BSMV-Pd nanorod diameters obtained from TEM characterization. The black dotted line shows the core diameter of BSMV (\sim 22 nm) while the red dashed line shows the core diameter of TMV (\sim 18 nm). (d) Diameters of primary Pd nanoparticles obtained at high q (q > 0.1). Data reduction and curve fitting were performed using Nika data reduction and Irena curve fitting software.

techniques, offered the unique opportunity to investigate a wide size range in a statistically significant way. This included both the populating Pd primary nanoparticle size and virion-Pd nanorod dimensions. The scattering relationship for the nanorods required a core—shell form factor incorporating scattering contrasts between Pd, carbon and water. A Guinier-Porod relationship was used to model the primary particles. Equations 1–7 describe the relevant scattering behavior for a unified curve fitting. 50,64,65

Figure 6a and Figure S2a show that the theoretical model reasonably describes the observed scattering behavior of the nanorods. Figure 6b and Figure S2b show the fitted scattering curves obtained from BSMV-Pd and TMV-Pd nanorods, respectively. From the volume fraction (Table S2) of Pd nanoparticles in solution, the Pd amount on the nanorods is observed to increase upon coating. The core diameter, which was modeled as a carbon tube, retains diameters of 22 nm, for BSMV, and 18 nm, for TMV, through all coatings. The estimated particle length of BSMV and TMV are 150 and 300 nm respectively, which agree with their published values. 40,41,55 Thus, the end-to-end aggregation of the nanorods which is evident in the TEM images of BSMV in Figure 2, is not statistically significant while nanorods are dispersed in solution. Figure 6c indicates that the shell thickness of Pd on BSMV increased during coating culminating in final diameters from 33.5 ± 3.3 nm to 47.0 ± 4.5 nm. However, this data (USAXS characterization) resulted in a slightly smaller estimation of the particle diameter compared with the TEM analysis obtained

from mean of diameters of 100 nanorods. Figure 5d shows that the primary Pd nanoparticles, which are packed on the viruses, are between 1 and 2 nm in diameter. This is in agreement with the distinguishable nanoparticle sizes observed after the partial coating of BSMV in Figure 3(a). Since, the primary particle sizes remain within this range as more coatings are added, it can be deduced that particle coalescence is minimal during coating. The display therefore consists of nonaggregating 1-2 nm particles along the 60 nm cylinder. This uniform active surface is uniquely useful for applications in catalysis, battery electrodes and further electroless deposition. Overall, the observed scattering behavior confirms the geometry and constituents of the synthesized nanorods in a statistically relevant way. To our knowledge, this is the first time that all size levels in a rod-like mineralized virus have been comprehensively and simultaneously analyzed.

CONCLUSIONS

BSMV has been introduced as a novel biotemplate for the formation of high quality Pd organic—inorganic nanorods in the absence of an exogenous reducer. The density of Pd on the nanorods could be tuned by repeated coating. Adsorption and reduction of $PdCl_3(H_2O)^-$ by BSMV were decoupled and individually examined. The virus surface mediated the reduction of $Pd^{(2+)}$ via first order kinetics in both $Pd^{(2+)}$ and BSMV, respectively. The adsorption equilibrium relationship of Pd on the BSMV surface was described by a multistep Langmuir isotherm suggesting an alternative and promising

mineralization, which takes advantage of both electrostatic and covalently driven affinity. The adsorption capacity of Pd species on BSMV is more than twice that on TMV. Both BSMV-Pd and TMV-Pd nanorods retain a consistent length and core diameter as they mediate formation of small 1-2 nm particles leading to rod diameters, which are controllable and monodisperse. Taken together, the nanomaterials synthesized on BSMV are of similar quality to those on TMV. BSMV also shows the potential to offer new kinds of mineralization possibilities via its native amino acid functional groups. This study has shown the viability and promise of BSMV as an alternate biotemplate for biomineralization of inorganic materials. Further work on this biotemplate will involve its genetic engineering, metallization with other metals, and exploration of selective inner channel mineralization to produce superfine nanowires.69

ASSOCIATED CONTENT

S Supporting Information

The Supporting Information is available free of charge on the ACS Publications website at DOI: 10.1021/acs.langmuir.6b03341.

Exposed amino acid sequences on the TMV and BSMV virus surfaces; low magnification TEM images of BSMV-Pd; TEM images of single TMV-Pd after incubation of 0.02 mg/mL of TMV in 0.75 mM of Na₂PdCl₄; USAXS experiments on TMV-Pd; obtained fitting parameters from core-shell scattering on BSMV-Pd and TMV-Pd; Obtained fitting parameters and particle diameter from Guinier—Porod scattering on Pd growing on BSMV and TMV (PDF)

AUTHOR INFORMATION

Corresponding Author

*E-mail: mtharris@purdue.edu.

ORCID

Oluwamayowa O. Adigun: 0000-0002-8317-4422

Notes

The authors declare no competing financial interest.

ACKNOWLEDGMENTS

Resources of the Advanced Photon Source (APS), a U.S. Department of Energy (DOE) Office of Science User Facility operated for the DOE Office of Science by Argonne National Laboratory (ANL) under Contract No. DE-AC02-06CH11357 were used in the experiments in this paper. USAXS data was collected at the 9-ID-C at the APS, ANL. XAS data was collected at the beamline 10ID-B at the APS, ANL, operated by MRCAT. MRCAT operations (General user proposal number: GU43567) are supported by the Department of Energy and the MRCAT member institutions. Zhenwei Wu, Evan Wegener, and Guanghui Zhang are acknowledged for their assistance with XAS experiments. Rohit Jaini is acknowledged for his useful remarks on the content of this article.

REFERENCES

- (1) Pochan, D. J.; Zhu, J.; Zhang, K.; Wooley, K. L.; Miesch, C.; Emrick, T. Multicompartment and Multigeometry Nanoparticle Assembly. *Soft Matter* **2011**, *7*, 2500.
- (2) Qiu, H.; Hudson, Z. M.; Winnik, M. A.; Manners, I. Multidimensional Hierarchical Self-Assembly of Amphiphilic Cylindrical Block Comicelles. *Science* **2015**, 347, 1329–1332.

(3) Lee, S.-Y.; Lim, J.-S.; Harris, M. T. Synthesis and Application of Virus-Based Hybrid Nanomaterials. *Biotechnol. Bioeng.* **2012**, *109*, 16–30.

- (4) Yang, C.; Choi, C. H.; Lee, C. S.; Yi, H. A Facile Synthesis-Fabrication Strategy for Integration of Catalytically Active Viral-Palladium Nanostructures into Polymeric Hydrogel Microparticles via Replica Molding. ACS Nano 2013, 7, 5032–5044.
- (5) Yang, C.; Manocchi, A. K.; Lee, B.; Yi, H. Viral Templated Palladium Nanocatalysts for Dichromate Reduction. *Appl. Catal., B* **2010**, 93, 282–291.
- (6) Yang, C.; Manocchi, A. K.; Lee, B.; Yi, H. Viral-Templated Palladium Nanocatalysts for Suzuki Coupling Reaction. *J. Mater. Chem.* **2011**, *21*, 187.
- (7) Yang, C.; Meldon, J. H.; Lee, B.; Yi, H. Investigation on the Catalytic Reduction Kinetics of Hexavalent Chromium by Viral-Templated Palladium Nanocatalysts. *Catal. Today* **2014**, 233, 108–116
- (8) Górzny, M. L.; Walton, A. S.; Wnęk, M.; Stockley, P. G.; Evans, S. D. Four-Probe Electrical Characterization of Pt-Coated TMV-Based Nanostructures. *Nanotechnology* **2008**, *19*, 165704.
- (9) Wnek, M.; Górzny, M. L.; Ward, M. B.; Wälti, C.; Davies, A. G.; Brydson, R.; Evans, S. D.; Stockley, P. G. Fabrication and Characterization of Gold Nano-Wires Templated on Virus-like Arrays of Tobacco Mosaic Virus Coat Proteins. *Nanotechnology* **2013**, *24*, 025605
- (10) Freer, A. S.; Gilpin, C.; Mueller, L.; Harris, M. A Novel Method to Determine the Resistance of Biotemplated Nanowires. *Chem. Eng. Commun.* **2015**, 202, 1216–1220.
- (11) Srinivasan, K.; Cular, S.; Bhethanabotla, V. R.; Lee, S. Y.; Harris, M. T. Nanomaterial Sensing Layer Based Surface Acoustic Wave Hydrogen Sensors. *IEEE Ultrason. Symp.* 2005 **2005**, 00, 645–648.
- (12) Bruckman, M. A.; Liu, J.; Koley, G.; Li, Y.; Benicewicz, B.; Niu, Z.; Wang, Q. Tobacco Mosaic Virus Based Thin Film Sensor for Detection of Volatile Organic Compounds. *J. Mater. Chem.* **2010**, *20*, 5715.
- (13) Mao, C.; Liu, A.; Cao, B. Virus-Based Chemical and Biological Sensing. *Angew. Chem., Int. Ed.* **2009**, *48*, *6790*–*6810*.
- (14) Jordan, P. C.; Patterson, D. P.; Saboda, K. N.; Edwards, E. J.; Miettinen, H. M.; Basu, G.; Thielges, M. C.; Douglas, T. Self-Assembling Biomolecular Catalysts for Hydrogen Production. *Nat. Chem.* **2015**, *8*, 179–185.
- (15) Tseng, R. J.; Tsai, C.; Ma, L.; Ouyang, J.; Ozkan, C. S.; Yang, Y. Digital Memory Device Based on Tobacco Mosaic Virus Conjugated with Nanoparticles. *Nat. Nanotechnol.* **2006**, *1*, 72–77.
- (16) Ma, Y.-Z.; Miller, R. a; Fleming, G. R.; Francis, M. B. Energy Transfer Dynamics in Light-Harvesting Assemblies Templated by the Tobacco Mosaic Virus Coat Protein. *J. Phys. Chem. B* **2008**, *112*, 6887–6892.
- (17) Miller, R. A.; Presley, A. D.; Francis, M. B. Self-Assembling Light-Harvesting Systems from Synthetically Modified Tobacco Mosaic Virus Coat Proteins. *J. Am. Chem. Soc.* **2007**, *129*, 3104–3109.
- (18) Lim, J. S.; Kim, S. M.; Lee, S. Y.; Stach, E. A.; Culver, J. N.; Harris, M. T. Biotemplated Aqueous-Phase Palladium Crystallization in the Absence of External Reducing Agents. *Nano Lett.* **2010**, *10*, 3863—3867
- (19) Freer, A. S.; Guarnaccio, L.; Wafford, K.; Smith, J.; Steilberg, J.; Culver, J. N.; Harris, M. T. SAXS Characterization of Genetically Engineered Tobacco Mosaic Virus Nanorods Coated with Palladium in the Absence of External Reducing Agents. *J. Colloid Interface Sci.* **2013**, 392, 213–218.
- (20) Lee, S. Y.; Royston, E.; Culver, J. N.; Harris, M. T. Improved Metal Cluster Deposition on a Genetically Engineered Tobacco Mosaic Virus Template. *Nanotechnology* **2005**, *16*, S435–S441.
- (21) Manocchi, A. K.; Horelik, N. E.; Lee, B.; Yi, H. Simple, Readily Controllable Palladium Nanoparticle Formation on Surface-Assembled Viral Nanotemplates. *Langmuir* **2010**, *26*, 3670–3677.
- (22) Manocchi, A. K.; Seifert, S.; Lee, B.; Yi, H. In Situ Small-Angle X-Ray Scattering Analysis of Palladium Nanoparticle Growth on

Tobacco Mosaic Virus Nanotemplates. *Langmuir* **2011**, 27, 7052–7058.

- (23) Lee, S. Y.; Choi, J.; Royston, E.; Janes, D. B.; Culver, J. N.; Harris, M. T. Deposition of Platinum Clusters on Surface-Modified Tobacco Mosaic Virus. *J. Nanosci. Nanotechnol.* **2006**, *6*, 974–981.
- (24) Shenton, W.; Douglas, T.; Young, M.; Stubbs, G.; Mann, S. Inorganic-Organic Nanotube Composites from Template Mineralization of Tobacco Mosaic Virus. *Adv. Mater.* **1999**, *11*, 253–256.
- (25) Dujardin, E.; Peet, C.; Stubbs, G.; Culver, J. N.; Mann, S. Organization of Metallic Nanoparticles Using Tobacco Mosaic Virus Templates. *Nano Lett.* **2003**, *3*, 413–417.
- (26) Lim, J.-S.; Kim, S.-M.; Lee, S.-Y.; Stach, E. a.; Culver, J. N.; Harris, M. T. Formation of Au/Pd Alloy Nanoparticles on TMV. *J. Nanomater.* **2010**, *2010*, 1–6.
- (27) Mao, C.; Solis, D. J.; Reiss, B. D.; Kottmann, S. T.; Sweeney, R. Y.; Hayhurst, A.; Georgiou, G.; Iverson, B.; Belcher, A. M. Virus-Based Toolkit for the Directed Synthesis of Magnetic and Semiconducting Nanowires. *Science* **2004**, *303*, 213–217.
- (28) Flynn, C. E.; Mao, C.; Hayhurst, A.; Williams, J. L.; Georgiou, G.; Iverson, B.; Belcher, A. M. Synthesis and Organization of Nanoscale II-VI Semiconductor Materials Using Evolved Peptide Specificity and Viral Capsid Assembly. *J. Mater. Chem.* **2003**, *13*, 2414.
- (29) Breitbart, M.; Rohwer, F. Here a Virus, There a Virus, Everywhere the Same Virus? *Trends Microbiol.* **2005**, *13*, 278–284.
- (30) Yang, C.; Jung, S.; Yi, H. A Biofabrication Approach for Controlled Synthesis of Silver Nanoparticles with High Catalytic and Antibacterial Activities. *Biochem. Eng. J.* **2014**, *89*, 10–20.
- (31) Bromley, K. M.; Patil, A. J.; Perriman, A. W.; Stubbs, G.; Mann, S. Preparation of High Quality Nanowires by Tobacco Mosaic Virus Templating of Gold Nanoparticles. *J. Mater. Chem.* **2008**, *18*, 4796.
- (32) Lim, H.-S.; Bragg, J. N.; Ganesan, U.; Ruzin, S.; Schichnes, D.; Lee, M. Y.; Vaira, A. M.; Ryu, K. H.; Hammond, J.; Jackson, A. O. Subcellular Localization of the Barley Stripe Mosaic Virus Triple Gene Block Proteins. *J. Virol.* **2009**, *83*, 9432–9448.
- (33) Bragg, J. N.; Jackson, A. O. The C-Terminal Region of the Barley Stripe Mosaic Virus Γb Protein Participates in Homologous Interactions and Is Required for Suppression of RNA Silencing. *Mol. Plant Pathol.* **2004**, *5*, 465–481.
- (34) Lim, H.-S.; Bragg, J. N.; Ganesan, U.; Lawrence, D. M.; Yu, J.; Isogai, M.; Hammond, J.; Jackson, A. O. Triple Gene Block Protein Interactions Involved in Movement of Barley Stripe Mosaic Virus. *J. Virol.* **2008**, 82, 4991–5006.
- (35) Donald, R. G.; Jackson, A. O. The Barley Stripe Mosaic Virus Gamma B Gene Encodes a Multifunctional Cysteine-Rich Protein That Affects Pathogenesis. *Plant Cell* **1994**, *6*, 1593–1606.
- (36) Jackson, A. O.; Lim, H.-S.; Bragg, J.; Ganesan, U.; Lee, M. Y. Hordeivirus Replication, Movement, and Pathogenesis. *Annu. Rev. Phytopathol.* **2009**, *47*, 385–422.
- (37) Makarov, V. V.; Skurat, E. V.; Semenyuk, P. I.; Abashkin, D. A.; Kalinina, N. O.; Arutyunyan, A. M.; Solovyev, A. G.; Dobrov, E. N. Structural Lability of Barley Stripe Mosaic Virus Virions. *PLoS One* **2013**, *8*, e60942.
- (38) Kendall, A.; Williams, D.; Bian, W.; Stewart, P. L.; Stubbs, G. Barley Stripe Mosaic Virus: Structure and Relationship to the Tobamoviruses. *Virology* **2013**, *443*, 265–270.
- (39) Clare, D. K.; Pechnikova, E. V.; Skurat, E. V.; Makarov, V. V.; Sokolova, O. S.; Solovyev, A. G.; Orlova, E. V. Novel Inter-Subunit Contacts in Barley Stripe Mosaic Virus Revealed by Cryo-Electron Microscopy. *Structure* **2015**, *23*, 1815–1826.
- (40) Harrison, B. D.; Nixon, H. L.; Woods, R. D. Lengths and Structure of Particles of Barley Stripe Mosaic Virus. *Virology* **1965**, *26*, 284–289.
- (41) Chiko, A. W. Evidence of Multiple Virion Components Mosaic in Leaf-Dip Virus Preparations of Barley Stripe. *Virology* **1975**, *63*, 115–122.
- (42) Kiselev, N. A.; Atabekov, I. G.; Kaftanova, A. S.; Novikov, V. K. Issledovanie Repolimerizatsii Virusnogo Belka I Resinteza Nekotorykh Palochkoobraznykh Virusov. *Biokhimiya* **1966**, *31*, *670*–*678*.

- (43) Kassanis, B.; Slykhuist, J. T. Some Properties of the Barley Stripes Virus. *Ann. Appl. Biol.* **1959**, 47, 254–263.
- (44) Jackson, A. O.; Brakke, M. K. Multicomponent Properties of Barley Stripe Mosaic Virus Ribonucleic Acid. *Virology* **1973**, *55*, 483–494
- (45) Drew Tait, C.; Janecky, D. R.; Rogers, P. S. Z. Speciation of Aqueous palladium(II) Chloride Solutions Using Optical Spectroscopies. *Geochim. Cosmochim. Acta* **1991**, *55*, 1253–1264.
- (46) Adigun, O. O.; Novikova, G.; Retzlaff-Roberts, E. L.; Kim, B.; Miller, J. T.; Loesch-fries, L. S.; Harris, M. T. Decoupling and Elucidation of Surface-Driven Processes during Inorganic Mineralization on Virus Templates. *J. Colloid Interface Sci.* **2016**, 483, 165.
- (47) Lim, J. S.; Kim, S. M.; Lee, S. Y.; Stach, E. A.; Culver, J. N.; Harris, M. T. Biotemplated Aqueous-Phase Palladium Crystallization in the Absence of External Reducing Agents. *Nano Lett.* **2010**, *10*, 3863–3867.
- (48) Ressler, T. WinXAS: A Program for X-Ray Absorption Spectroscopy Data Analysis under MS-Windows. *J. Synchrotron Radiat.* **1998**, *5*, 118–122.
- (49) Ilavsky, J.; Zhang, F.; Allen, A. J.; Levine, L. E.; Jemian, P. R.; Long, G. G. Ultra-Small-Angle X-Ray Scattering Instrument at the Advanced Photon Source: History, Recent Development, and Current Status. *Metall. Mater. Trans. A* **2013**, *44*, 68–76.
- (50) Guinier, A.; Fournet, G. Small Angle Scattering of X-rays; John Wiley and Sons: New York, 1955.
- (51) Kline, S. R. Reduction and Analysis of SANS and USANS Data Using IGOR Pro. *J. Appl. Crystallogr.* **2006**, *39*, 895–900.
- (52) Boily, J.-F.; Seward, T. M. Palladium(II) Chloride Complexation: Spectrophotometric Investigation in Aqueous Solutions from 5 to 125°C and Theoretical Insight into Pd-Cl and Pd-OH2 Interactions. *Geochim. Cosmochim. Acta* **2005**, *69*, 3773–3789.
- (53) Tan, Y. N.; Lee, J. Y.; Wang, D. I. C. Uncovering the Design Rules for Peptide Synthesis of Metal Nanoparticles. *J. Am. Chem. Soc.* **2010**, 132, 5677–5686.
- (54) Virus Taxonomy: Eighth Report of the International Committee of Taxonomy of Viruses; Fauchet, C., Mayo, M., Maniloff, J., Desselberger, U., Ball, L., Eds.; Elsevier Academic Press: San Diego, 2005.
- (55) Alonso, J. M.; Górzny, M. Ł.; Bittner, A. M. The Physics of Tobacco Mosaic Virus and Virus-Based Devices in Biotechnology. *Trends Biotechnol.* **2013**, *31*, 530–538.
- (56) Yao, Y.; Lenhoff, A. M. Electrostatic Contributions to Protein Retention in Ion-Exchange Chromatography. 2. Proteins with Various Degrees of Structural Differences. *Anal. Chem.* **2005**, *77*, 2157–2165.
- (57) Patwardhan, S. V.; Emami, F. S.; Berry, R. J.; Jones, S. E.; Naik, R. R.; Deschaume, O.; Heinz, H.; Perry, C. C. Chemistry of Aqueous Silica Nanoparticle Surfaces and the Mechanism of Selective Peptide Adsorption. *J. Am. Chem. Soc.* **2012**, *134*, 6244–6256.
- (58) Maruyama, T.; Matsushita, H.; Shimada, Y.; Kamata, I.; Hanaki, M.; Sonokawa, S.; Kamiya, N.; Goto, M. Proteins and Protein-Rich Biomass as Environmentally Friendly Adsorbents Selective for Precious Metal Ions. *Environ. Sci. Technol.* **2007**, *41*, 1359–1364.
- (59) Czinkota, I.; Földényi, R.; Lengyel, Z.; Marton, A. Adsorption of Propisochlor on Soils and Soil Components Equation for Multi-Step Isotherms. *Chemosphere* **2002**, *48*, 725–731.
- (60) Konda, L. N.; Czinkota, I.; Fuleky, G.; Morovján, G. Modeling of Single-Step and Multistep Adsorption Isotherms of. *J. Agric. Food Chem.* **2002**, *50*, 7326–7331.
- (61) Cruywagen, J. J.; Kriek, R. J. Complexation of palladium(II) with Chloride and Hydroxide. J. Coord. Chem. 2007, 60, 439-447.
- (62) Kirik, S. D.; Solovyov, L. A.; Blokhin, A. I.; Yakimov, I. S.; Blokhina, M. L. Structures and Isomerization in diamminedichloropalladium(II). *Acta Crystallogr., Sect. B: Struct. Sci.* 1996, 52, 909–916.
- (63) Ho Kim, Y.; Nakano, Y. Adsorption Mechanism of Palladium by Redox within Condensed-Tannin Gel. *Water Res.* **2005**, *39*, 1324–1330.
- (64) Beaucage, G.; Schaefer, D. W. W. Structural Studies of Complex Systems Using Small-Angle Scattering: A Unified Guinier/power-Law Approach. *J. Non-Cryst. Solids* **1994**, *172–174*, 797–805.

(65) Beaucage, G. Approximations Leading to a Unified Exponential/Power-Law Approach to Small-Angle Scattering. *J. Appl. Crystallogr.* **1995**, 28, 717–728.

- (66) Ilavsky, J.; Jemian, P. R.; Allen, A. J.; Zhang, F.; Levine, L. E.; Long, G. G. Ultra-Small-Angle X-Ray Scattering at the Advanced Photon Source. *J. Appl. Crystallogr.* **2009**, *42*, 469–479.
- (67) Ilavsky, J. Nika: Software for Two-Dimensional Data Reduction. J. Appl. Crystallogr. **2012**, 45, 324–328.
- (68) Ilavsky, J.; Jemian, P. R. Irena: Tool Suite for Modeling and Analysis of Small-Angle Scattering. *J. Appl. Crystallogr.* **2009**, 42, 347–353.
- (69) Zhou, K.; Zhang, J.; Wang, Q. Site-Selective Nucleation and Controlled Growth of Gold Nanostructures in Tobacco Mosaic Virus Nanotubulars. *Small* **2015**, *11*, 2505–2509.
- (70) Madej, T.; Lanczycki, C. J.; Zhang, D.; Thiessen, P. A.; Geer, R. C.; Marchler-bauer, A.; Bryant, S. H. MMDB and VAST+: Tracking Structural Similarities between Macromolecular Complexes. *Nucleic Acids Res.* **2014**, *42*, D297–D303.